SUPPORTING MATERIAL FOR

Stochastic fusion simulations and experiments suggest passive and active roles of hemagglutinin during membrane fusion

Donald W. Lee,* Vikram Thapar,* Paulette Clancy and Susan Daniel[#]

School of Chemical and Biomolecular Engineering

Cornell University, Ithaca, NY 14853

Overview

This supporting material provides additional details on prior literature, microfluidic preparation, fusion assay setup, fluorescence recovery after photobleaching (FRAP) experiments, extents of fusion, a list of species used in simulation, calculation of "hopping rate" for species diffusion in the simulation, refining the k_{bend} values, the fusible unit species tested by simulation, our simulation algorithm, flow chart of simulation strategy, and a sensitivity analysis of slopes of log V_{max} vs log [$HA_{1,2}$] plots.

Summary of literature work

The minimal number of HA trimers necessary for membrane fusion, w, and the minimal number of activated HA trimers required, q, have been debated for more than two decades. Table S1 is a summary of past work related to this topic, together with the authors' original hypothesis or conclusions for suitable values of w and q. Each work has been classified according to the experimental approach used to determine w and q, as described in the table caption. Note that many previous studies did not consider w and q as separate parameters, which is why w and q often appear as the same value in the table.

Year	Authors	Approach	*w*	*q*	Fitting Method	Source of HA trimer	Fusion Exp. or Simulation
1986	Gibson et al.	Var F	1	1	Multiple-Hit-Multiple-Target Model	A/PR/8/34 (H1N1)	Virus-Vesicle
1987	Bundo-Morita et al.	Var F	1	1	Multiple-Hit-Multiple-Target Model	A/PR/8/34 (H1N1)	Virus-Vesicle
1990	Ellens et al.	Var FB	2-5	2-5	N/A	A/Japan/305/57 (H2N2)	Cell-Vesicle
1990	Stegmann et al.	Const. FB	> 1	> 1	N/A	X-31 A/Aichi/68 (H3N2)	Virus-Vesicle
1996	Danieli et al.	Var FB	3-4	3-4	Hill Equation	A/Japan/305/57 (H2N2)	Cell-Cell
1996	Blumenthal et al.	Const FB	6	6	Power Law	A/Japan/305/57 (H2N2)	Cell-Cell
2000	Günther-Ausborn et al.	Var F	1	1	$V_{initial} = k[HA_{1,2}]^q$	A/Shangdong (H3N2) X-47 (H3N2)	Virosome-Cell
2000	Bentz	Var FB + Const FB	> 8	2-3	Mass Action Kinetic Model	A/Japan/305/57 (H2N2)	Cell-Cell
2001	Schreiber et al.	Var FB + Const FB	3	3	Simulation	A/Japan/305/57 (H2N2)	Cell-Cell
2006	Imai et al.	Var F Var FB	1 > 1	1 > 1	$V_{max} = k[HA_{1,2}]^q$	A/PR/8/1934 (H1N1)	Virosome-Cell
2008	Floyd et al.	Const FB	3	3	Gamma Distribution	X-31 A/Aichi/68 (H3N2)	Virus-SLB
2011	Dobay et al.	Const FB	6	3	Simulation	A/PR/8/1934 (H1N1) X-31 A/Aichi/68 (H3N2)	Virus-SLB
2012	Costello et al.	Const FB	≤ 2	≤ 2	Gamma Distribution	X-31 A/Aichi/68 (H3N2)	Virus-SLB
2013	Ivanovic et al.	Const FB	3-4	3-4	Gamma Distribution & Simulation	A/Udorn/62 (H3N2) X-31 A/Aichi/68 (H3N2)	Virus-SLB
2013	Lee et al. (this work)	Var F + Var FB + Const FB	3	1	Simulation	A/PR/8/1934 (H1N1) X-31 A/Aichi/68 (H3N2)	Virosome-Cell Virus-SLB

TABLE S1 Chronological list of experiments related to determining *w* or *q*. Variable F (var F) varies the fraction of fusogenic HA trimers at a constant total HA density. Variable FB (var FB) varies the total density of fusogenic HA trimers. Constant FB (const FB) does not vary HA density and extracts *w* or *q* by fitting fusion lag time data to statistical models. The reported *w* and *q* values from listed studies were interpreted from the original references and not obtained through simulations performed in this work.

Microfluidic preparation

The microfluidic devices used for fusion experiments were prepared according to the following procedure. Glass coverslip slides (No. 1.5 thickness) [VWR, Radner, PA] were cleaned for 10 min using a piranha solution consisting of 45 mL of 50% hydrogen peroxide [Sigma-Aldrich, St. Louis, MO] and 105 mL of sulfuric acid [VWR, Radner, PA]. Cleaned glass slides were rinsed and stored in deionized water. A polydimethylsiloxane (PDMS) [Dow Corning, Midland, MI] mold of microfluidic channels was prepared using a patterned silica wafer made through photolithography. The microfluidic channel dimensions are 135 μm wide, 75 μm deep, and 1.5 cm long. A glass slide and PDMS mold were annealed together after a 30-second oxygen plasma cleaning step. Tygon tubes (0.02”ID x 0.06”OD) [Saint-Gobain Performance Plastic, Worcester, MA] were attached to the microfluidic device to facilitate the loading of various solutions into the channels. The microfluidic device is shown in Fig. S1.

Images of fusion assay and sample hemifusion event

Fig. S1 shows a picture of the microfluidic device and schematic drawing of the fusion assay setup. A sample image sequence of a fusing virus is also shown. The intensity traces of the membrane dye (R18) in the virus and the acid-sensitive membrane dye (Oregon Green) in the target membrane are used to determine the hemifusion lag time for an individual virion.

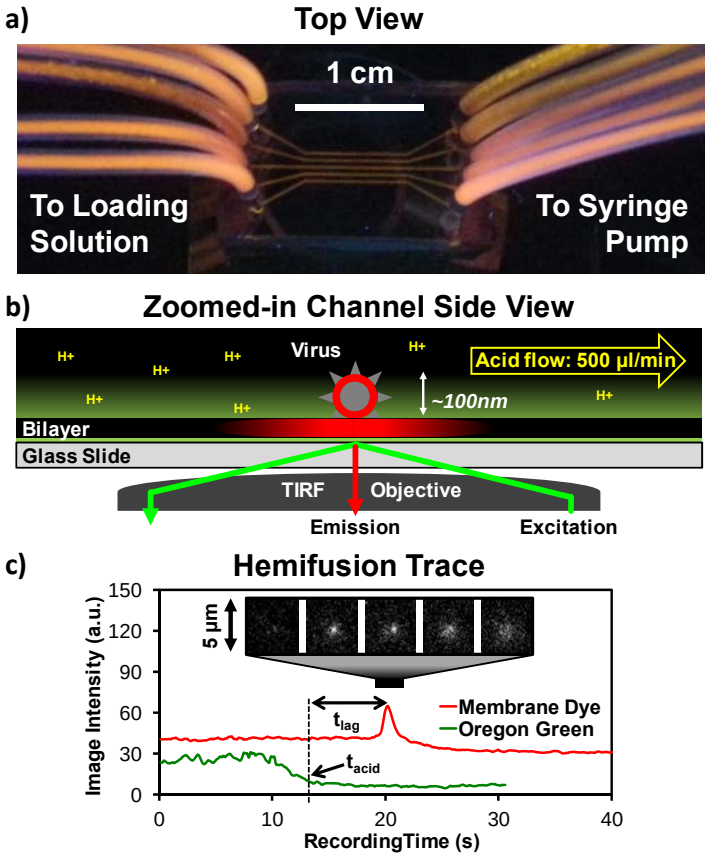

FIGURE S1 Virus fusion assay setup and sample hemifusion trace. (a) Photo of a typical microfluidic device. Channels were filled with fluorescent dye for visualization purposes. (b) Schematic diagram of a microfluidic channel used in experiments. A dye-labeled virus is shown fusing to a supported lipid bilayer (SLB) upon an acid trigger, inside a channel. Total internal reflection fluorescence (TIRF) microscopy is used to observe the fusion events. (c) Sample virus fusion images and hemifusion trace showing how the hemifusion lag time, t_{lag}, is determined.

Fluorescence recovery after photobleaching (FRAP) experiments

The mobility of the target membranes were determined using FRAP. The target membranes were labeled with R18 membrane fluorophores by adding 0.5 µL of 1.8 mM R18 in ethanol solution to 500 µL of lipid A or lipid B vesicle solutions. The solutions were sonicated for 30 min before loading them into microfluidic channels to form supported lipid bilayers (SLBs), which were allowed to form over the course of 20 min. Channels with SLBs were rinsed with citric acid buffer set at pH 3.0, 3.5, 4.0, or 4.5. The bilayer was illuminated with a 561 nm

wavelength light source. A 16 μm-diameter circular area in the bilayer was photobleached with a 5 mW, 561 nm wavelength Gaussian laser for 3 seconds. Video images of the bilayer were recorded before and after photobleaching, and the mean intensity of the bleached spot over time was measured. Another area that has not been photobleached, the reference spot (see Fig. S2), was monitored to correct for global photobleaching caused by the microscope light source. The normalized mean intensity of the photobleached region, $f_k(t)$, was determined according to the following equation:

$$f_k(t) = \frac{[F_k(t) - F_c(t)] - [F_k(0) - F_c(0)]}{[F_k(-\infty) - F_c(-\infty)] - [F_k(0) - F_c(0)]}$$

where $F_k(t)$ and $F_c(t)$ are the fluorescence intensities at time t of the bleached and reference spot, respectively. The time immediately after photobleaching is $t = 0$, and the time before photobleaching is $t = -\infty$. The methods of Axelrod et al. (1) were used to fit the fluorescence recovery data and extract the characteristic time for diffusion, t_d, for a bleach spot made from a Gaussian laser. The diffusion coefficient was calculated as $D = r^2/(4t_d)$, where r is the radius of the laser beam at e^{-2} laser intensity height. D values for R18 fluorophores in SLB A are shown in Fig. 5b of the main report.

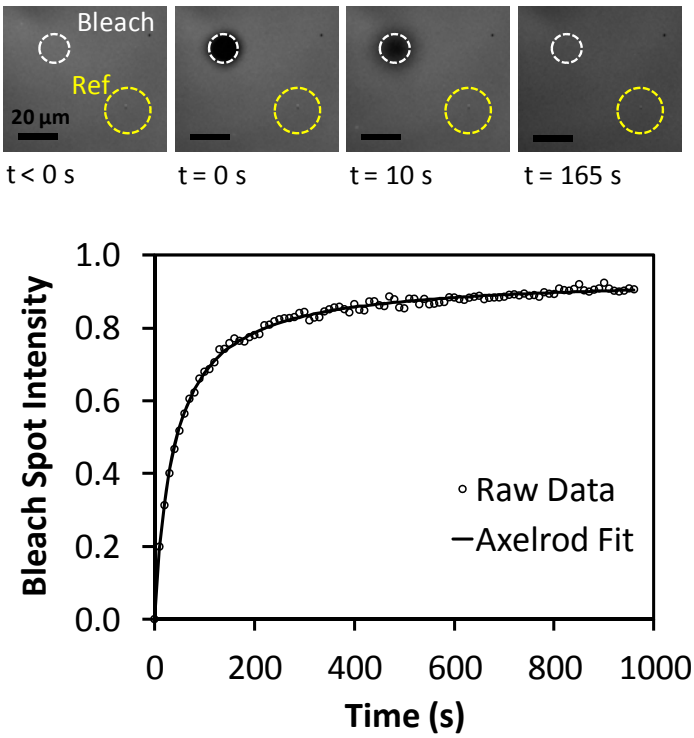

FIGURE S2 A representative FRAP recovery curve used to determine diffusion coefficient in supported bilayers. (Top) Image sequence of a R18-labeled supported lipid bilayer with LPC lipid (SLB B) at pH 4.5. The mean intensity of the photobleached circular region (white dotted circle) is tracked and compared with a reference region (yellow dotted circle) that has not been photobleached. (Bottom) the normalized intensity of the bleached spot is plotted with time and fitted to the diffusion equation derived by Axelrod et al. (1) to extract the characteristic time for diffusion, t_d. For this example, the bleach spot radius, r, is 8.13 µm and t_d is 36 s. The calculated D is 0.46 µm^2/s.

Extents of fusion of experimental data

The fraction of bound viruses that fused was tracked to verify that protein denaturation and subsequent loss of function due to acidification is negligible in the range of pH employed in these studies. An in-house particle counting program was developed in MATLAB to detect and count fluorescently-labeled virus particles by identifying high-intensity spots that have a circular morphology. Extent of fusion is defined as the number of viruses that fused divided by the total number of viruses observed. Fig. S3 show the resulting extents of fusion at various pH conditions for triggering fusion. The consistent fusion extents across the tested pH range suggest that the virions were similarly functional across the experiments, and also that acid-induced

denaturation of HA trimers is not occurring across the pH range. This result is also in agreement with studies by Doms et al. in 1985 (2), who investigated acid-induced denaturation of HA trimers.

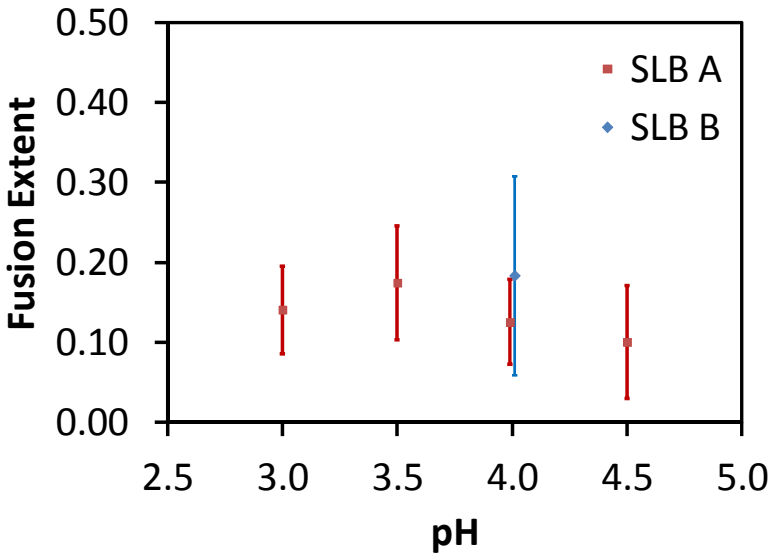

FIGURE S3 Extent of fusion for the X31 virus as the pH is varied in the range 3.0-4.5. The extent of fusion in this range is essentially the same within the uncertainty in the data.

List of species used in simulation

Table S2 is a list of all species used in the simulation, with their description and allowable locations in the simulation space. Species that are physically associated with both the viral and host membrane are only allowed in the contact area region.

Outside the contact area, only HA_0, $HA_{1,2}$, $HA_{1,2}^*$, and *R* are mobile species. Inside the contact area, any HA trimers that are physically interacting with the target membrane or receptor are treated as immobile species. Unbound HA_0 and unbound *R* remain mobile inside the contact area. Table S2 summarizes the mobility of species.

Symbol	Description	Allowed Location	Mobility
R	Sialic acid receptor	Anywhere	Mobile
$HA_{1,2}$	Fusogenic $HA_{1,2}$ trimer	Anywhere	Mobile
HA_0	Non-fusogenic HA_0 trimer	Anywhere	Mobile
$HA_{1,2}$-*R* HA_0-*R* $HA_{1,2}$*-*R*	An HA trimer that is bound to R	Contact Area	Immobile
$HA_{1,2}$*	Conformationally changed $HA_{1,2}$	Anywhere	Immobile inside contact area. Mobile elsewhere.
Fusible Unit	An arrangement of HA trimers that can bend the target bilayer.	Contact Area	N/A
Bent Complex	A bent state of the target bilayer, which precedes hemifusion.	Contact Area	Immobile
Hemifusion Stalk	A merged state of the virus and target bilayer.	Contact Area	Immobile

TABLE S2 Summary of the species involved in the simulations.

Calculation of "hopping rate" for species diffusion in the simulation

The only diffusive species in our simulation are receptors, *R*, and HA trimers, HA_0, $HA_{1,2}$, or $HA_{1,2}^*$. A diffusion event is defined as the migration of a molecule from one grid element to a neighboring grid element. This is modeled as a unimolecular reaction (3), where the hopping rate parameter is related to the macroscopic diffusion coefficient *D* through the relation $k_{diff} = nD/h^2$, where *h* is the center to center distance between two adjacent grid elements, and *n* is 2/3 for a hexagonal lattice system (4-5). The diffusion coefficients for HA and glycoprotein receptor were estimated from existing FRAP experiments by Danieli et al. (6) and Sheetz (7), respectively. The hopping rate for HA, $k_{diff,HA}$, was calculated as 740 s^{-1}, while that for the glycoprotein is 74 s^{-1}. We assumed that the viruses studied by Imai et al. were attached to the glyocoprotein on the ghost red blood cell membranes. As for our own experiments, the viruses were bound to a different receptor called GD_{1a}, a glycolipid with sialic acid groups. The diffusion coefficient for $GD_{1a}$was estimated at 1 $\mu m^2/s$ based on the diffusion coefficient of the

lipid fluorophore, R18. However, the calculated hopping rate for GD_{1a}, $k_{diff,R}$,is 24,700 s^{-1}, which is many orders of magnitude greater than other rate parameters in the simulation. The simulation algorithm (discussed in detail below) will simulate each reaction event according to their reaction propensities, and therefore GD_{1a} diffusion would dominate the most of the simulation processing power. To prevent this from happening, we have capped $k_{diff,R}$ for GD_{1a} at 2000 s^{-1}.

Refining k_{bend} values

To refine the k_{bend} values starting with $k_{bend,approx}$, the bootstrap method (8) is used. In this method, the k_{bend} parameter is varied at 10 evenly spaced values in the interval [$0.8k_{bend,approx}$, $1.2k_{bend,approx}$] in which 3000 simulations are performed for each k_{bend} value. In one iteration of refinement, 500 random lag times from each distribution for each k_{bend} value are compared to the actual lag time distribution through a KS test. The simulated distribution with the smallest KS statistic (D_{test}) is determined, and the k_{bend} value for that distribution is stored. This iteration is performed for a total of 6 times to find the mean and standard deviation of these stored k_{bend} values. In the main text, any k_{bend} values with their error bars reported have been refined using this procedure.

Fusible unit species tested by simulation

A fusible unit is defined by an arrangement of HA trimers in adjacent grid elements. At least q number of HA trimers must be pH-activated and the relative locations of the pH-activated and un-activated HA trimers do not matter within the fusible unit perimeter, highlighted by a thick blue line in Fig. S4. Other configurations of fusible units for different combinations of w and q are shown below in Fig. S4.

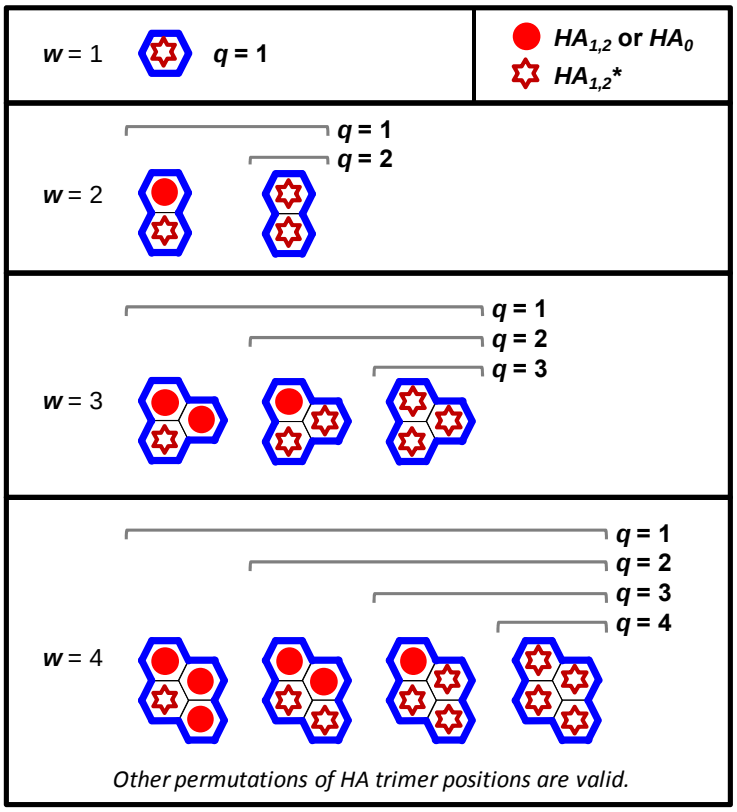

FIGURE S4 Fusible unit species studied in this simulation. A fusible unit is defined as a localized group of hexagonal lattice grid elements that contain *w* HA trimers, regardless of conformational state, and at least *q* activated HA trimers. Permutations of the positions of HA trimers within the blue fusible unit perimeter do not matter when defining a fusible unit species.

Simulation algorithm

Stochastic fusion simulations are performed using the following iterative procedure.

1) Initialize the system at time $t = 0$, which corresponds to the time at which the system is acidified.

2) Calculate the propensity, $a(t)$, of all molecular events using the relation $a_i(t) = k_i G_i(t)$, where k_i is the rate parameter of event i and $G_i(t)$ is the number of species involved, which

here would be the number hexagonal lattice grid elements (or groups of elements) containing those species.

3) Select a random molecular event j by finding the minimum j value that satisfies $\frac{\sum_{j'=1}^{j} a_{j'}(t)}{a_0(t)} \geq r_1$, where $a_0(t)$ is the total propensity of all events and r_1 is a uniform random number in an interval [0,1].

4) Calculate time step, τ, using the relation $\tau = \frac{1}{a_0} \ln\left(\frac{1}{r_2}\right)$, where r_2 is a uniform random number in an interval [0,1].

5) Advance the simulated time, t, by τ and update the population/location of species in the simulation based on the chosen event.

6) Repeat steps 2 through 5 until a terminating event occurs. Our termination events were the formation of a hemifusion stalk species or a simulated time of t = 5 min.

Flow chart of simulation strategy

The flow chart in Fig. S5 summarizes the strategy used to determine the unknown parameters (w, q, and k_{bend}) and also to validate the model. More details are provided in the Main Text in the section titled "Strategy Overview for Determining w and q."

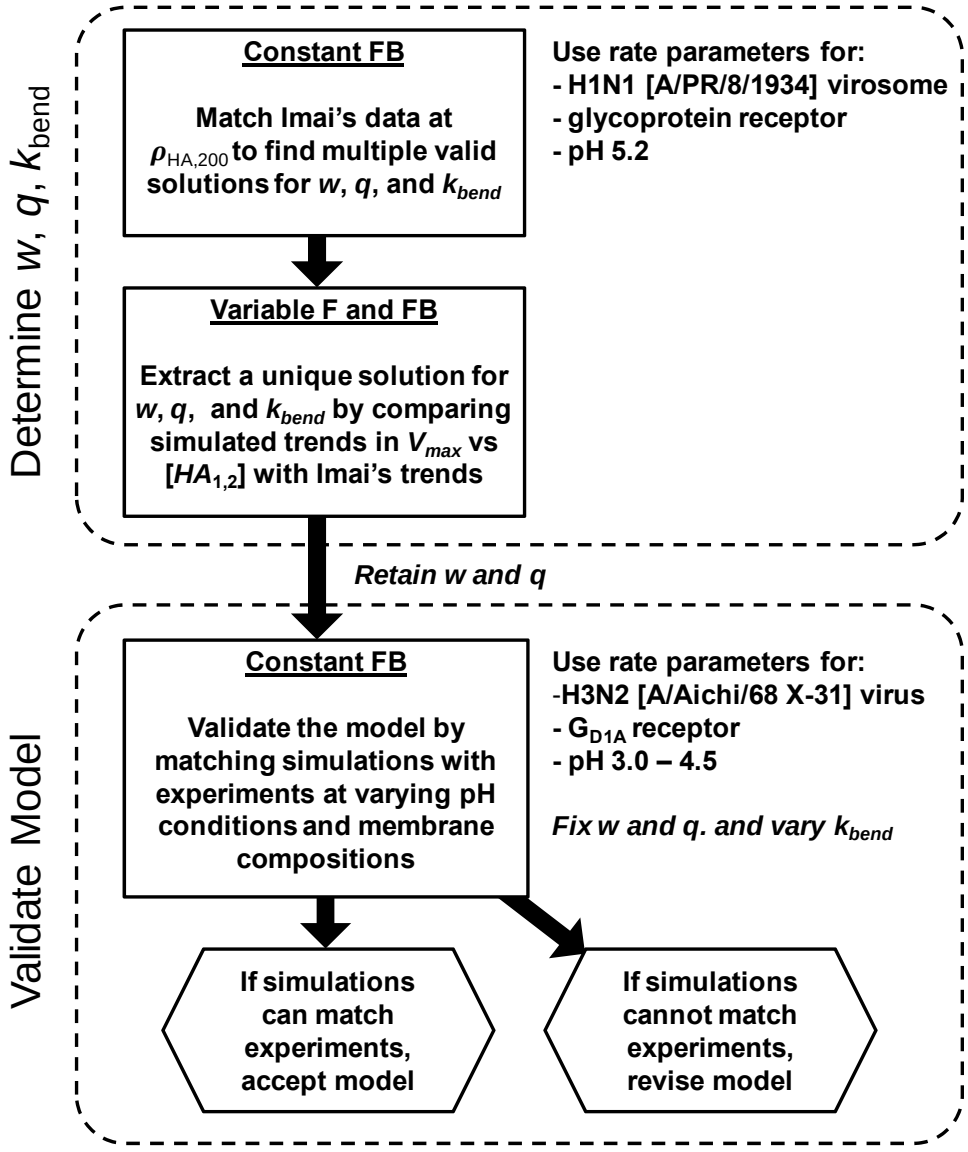

FIGURE S5 Flow diagram of the simulation process used to determine values for k_{bend}, w, and q.

Sensitivity analysis of slopes of log V_{max} vs log [$HA_{1,2}$] plots

We performed two types of sensitivity analysis to illustrate the robustness of our model in determining w and q. In the first analysis, we repeated the Variable F and FB simulations at two other contact areas to ensure that w and q values were dependent on our original choice of contact area size. The slopes of plots of log V_{max} vs log [$HA_{1,2}$] for both Variable F and FB simulations did not change significantly for 8×8, 10×10, and 14×14 grid sizes for the contact

area. Thus, our conclusions regarding optimal w and q values are not affected by the choice of contact area size (Fig. S6). We note that the choice of contact area size does alter the k_{bend} values obtained by matching with Imai et al.'s distribution at $\boldsymbol{\rho}_{\mathrm{HA},200}$. A larger contact area increases the rate of fusion, which is compensated by a lower k_{bend} value in order to match experimental data. We thus emphasize that our numerical rate value reported for k_{bend} is based on the contact area being 2338 nm^2 (which is equivalent to 10x10 hexagonal grid elements), and that it scales directly with contact area size.

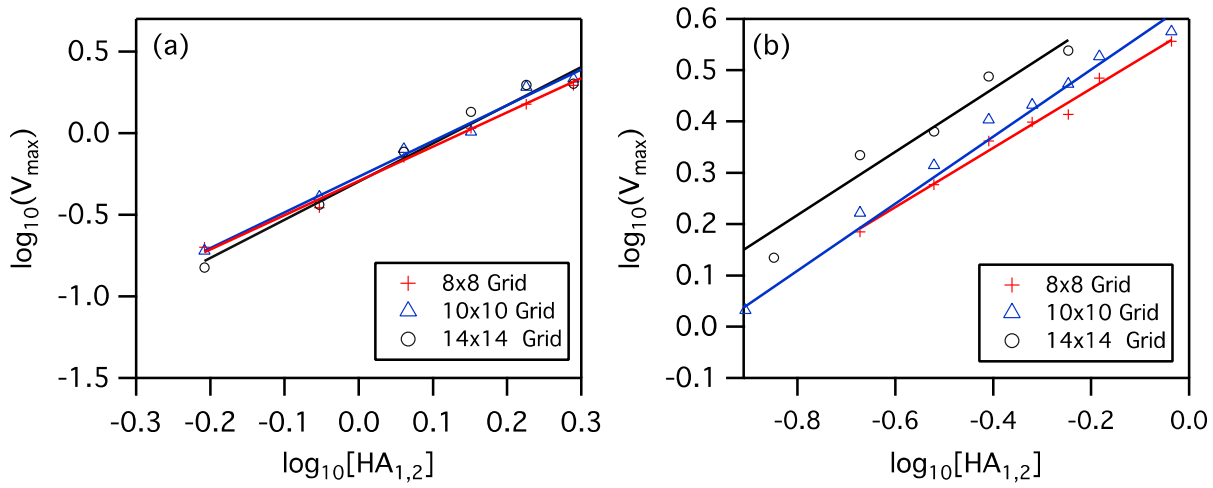

FIGURE S6 Insensitivity of slopes of log V_{max} vs log [$HA_{1,2}$] to choice of contact area size, for w = 3, q = 1, and k_{act} = 0.067 s^{-1}. (a) Results from Variable FB simulations. The slopes of the best-fit lines are 2.09 (r^2 = 0.99), 2.19 (r^2 = 0.99) and 2.34 (r^2 = 0.99) for contact area sizes of 8×8, 10×10, and 14×14 grid elements, respectively. (b) Results from Variable F simulations. The slopes of the best-fit lines are 0.58 (r^2 = 0.98), 0.65 (r^2 = 0.99) and 0.62 (r^2 = 0.97) for contact area sizes of 8×8, 10×10, and 14×14 grid elements, respectively. The HA density, [$HA_{1,2}$], has been converted to its corresponding mass ratio of HA to lipid in this plot to be consistent with Imai et al.'s studies (9). The $k_{bend,\ approx}$ values determined from the fits are 0.078 s^{-1}, 0.05 s^{-1}, and 0.0255 s^{-1} for the 8x8, 10x10, and 14x14 contact area sizes, respectively.

In the second analysis, we repeated the Variable F and FB simulations at another k_{act} value to ensure that this parameter did not change our choice of values for w and q. We performed this analysis because we do not know the rate of conformational change for the HA

trimers in the H1N1 influenza virus used by Imai et al. (9). We began by using a value for k_{act} of 0.067 s^{-1}, which is the HA activation rate for X31 virus (H3N2) at pH 5.2, the pH value used by Imai et al. For a second value, we chose an arbitrary k_{act} value of 0.01 s^{-1}. Variable F and FB simulations were run for both cases of k_{act} using the same procedure described in the main manuscript. Despite an almost order of magnitude difference in k_{act}, the slopes of the log V_{max} vs log [$HA_{1,2}$] plots did not change, as shown in Fig. S7. In the main manuscript, we also showed that using a k_{act} value of 5.2 s^{-1} did not require us to change w and q when studying fusion kinetics at pH values below 4.5 and with different membrane compositions. Taken together, these results suggest that w and q is insensitive to the choice of k_{act} value, at least within the range of 0.01 and 0.067 s^{-1} studied here.

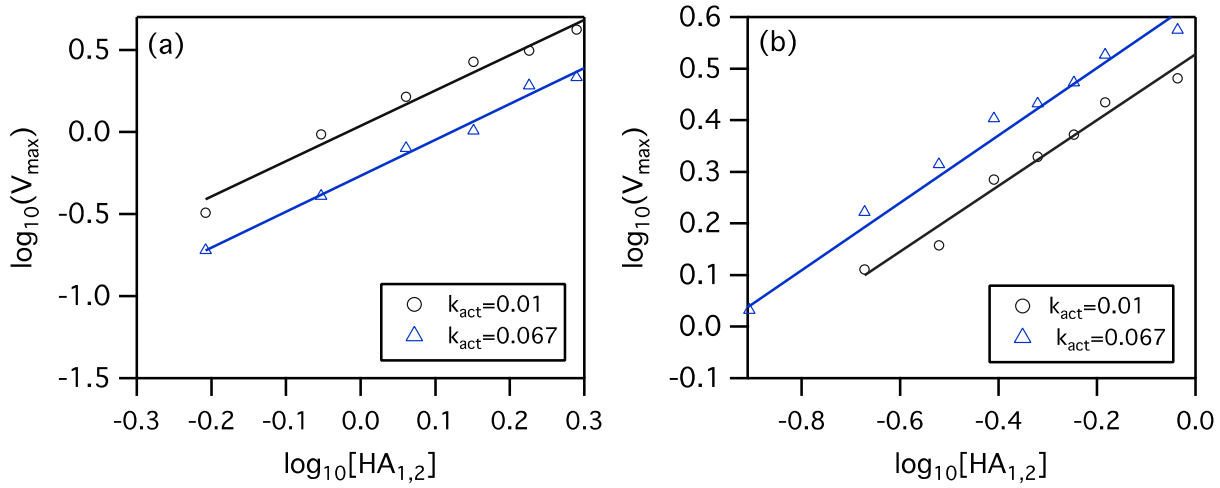

FIGURE S7 Insensitivity of slopes of log V_{max} vs log [$HA_{1,2}$] to the choice of k_{act}, for w = 3, q = 1, and contact area = 10x10 grid size (2338 nm^2). a) Results from Variable FB simulations. The slopes of the best-fit lines are 2.19 (r^2 = 0.99) and 2.23 (r^2 = 0.98) when k_{act} is 0.067 and 0.01 s^{-1}, respectively. b) Results from Variable F simulations. The slopes of the best-fit lines are 0.65 (r^2 = 0.99) and 0.62 (r^2 = 0.98) when k_{act} is 0.067 and 0.01 s^{-1} respectively. The HA density, [$HA_{1,2}$], has been converted to its corresponding mass ratio of HA to lipid in this plot to be consistent with Imai et al. (9). The $k_{bend,\ approx}$ values from the fits are 0.28 and 0.05 $s^{-1}$for k_{act} values of 0.01 and 0.067 s^{-1}, respectively.

SUPPORTING REFERENCES

1. Axelrod, D., D.E. Koppel, J. Schlessinger, E. Elson, and W.W. Webb. 1976. Mobility measurement by analysis of fluorescence photobleaching recovery kinetics. BIOPHYS J. 16:1055-1069.
2. Doms, R.W., A. Helenius, and J. White. 1985. Membrane fusion activity of the influenza virus hemagglutinin. The low pH-induced conformational change. J BIOL CHEM. 260:2973-2981.
3. Bernstein, D. 2005. Simulating mesoscopic reaction-diffusion systems using the Gillespie algorithm. PHYS REV E. 71:041103.
4. Arjunan, S. and M. Tomita. 2010. A new multicompartmental reaction-diffusion modeling method links transient membrane attachment of E. coli MinE to E-ring formation. SYST SYNTH BIOL. 4:35-53.
5. Klein, A.M., V. Nikolaidou-Neokosmidou, D.P. Doupé, P.H. Jones, and B.D. Simons. 2011. Patterning as a signature of human epidermal stem cell regulation. J ROY SOC INTERFACE. 8:1815-1824.
6. Danieli, T., S.L. Pelletier, Y.I. Henis, and J.M. White. 1996. Membrane fusion mediated by the influenza virus hemagglutinin requires the concerted action of at least three hemagglutinin trimers. J CELL BIOL. 133:559-569.
7. Sheetz, M.P. 1983. Membrane skeletal dynamics: role in modulation of red cell deformability, mobility of transmembrane proteins, and shape. SEMIN HEMATOL. 20:175-188.
8. Efron, B. and R. Tibshirani, *An introduction to the bootstrap*. Vol. 57. 1993: CRC press.
9. Imai, M., T. Mizuno, and K. Kawasaki. 2006. Membrane fusion by single influenza hemagglutinin trimers. J BIOL CHEM. 281:12729-12735.